Biophysical Chemistry 14 (1981) 111–122
Elsevier/North-Holland Biomedical Press

X-RAY EQUATORIAL ANALYSIS OF CRAB STRIATED MUSCLE IN THE RELAXED AND RIGOR STATES

Katsuzo WAKABAYASHI and Keiichi NAMBA

Department of Biophysical Engineering, Faculty of Engineering Science, Osaka University, Toyonaka, Osaka 560, Japan

Received 13 March 1981
Revised manuscript received 27 May 1981

The structure of muscle projected along the fiber axis was studied by equatorial X-ray diffraction. The electron-density distributions in axial projection of muscle were derived by the Fourier syntheses to a resolution of 7 nm in the relaxed and rigor states. The structure of the thick filament backbone (diameter about 21.5 nm) has a nearly smooth cylindrical surface and a low electron-density core (diameter about 7 nm) in the center. In the relaxed state, the center of gravity of the myosin heads is situated at a radius of 19.6 nm from the center of the thick filament, lying just between the surface of the thick filament backbone and the surface of the thin filament (diameter about 8.4 nm). From the electron-density distributions in two states, the amount of mass transfer from the thick filament to the thin filament was estimated. It was in accordance with that predicted from the structure derived by the X-ray layer-line analyses.

Introduction

X-ray diffraction studies have been carried out extensively on vertebrate striated muscles, insect flight muscle and some crustacean striated muscles. The diffraction patterns from these muscles have several common features. In the relaxed state, the layer-line reflections due to the thick filaments are distinct, suggesting a regular arrangement of myosin projections around the thick filament [1–4]. In the rigor state, the layer-line reflections due to the thick filaments are weakened and those due to the thin filament become intense, indicating that myosin projections attach to the thin filaments. Recently, several workers have reported that myosin projections attach periodically to the thin filaments in the rigor state of insect flight muscle [5] and crustacean muscles [4,6–8]. In the equatorial diffraction patterns, the intensity ratio of the 1,0 to the 1,1 or the (1,1 + 2,0) reflections indexed on the hexagonal filament lattice decreases when the muscle changes from the relaxed to the rigor state (e.g. ref. [9]) and during contraction (e.g. ref. [10]). This decrease is concerned with the mass transfer from the thick filament to the thin filament and has been interpreted in terms of the movement of myosin projections where they can attach to and interact with the thin filaments [9,10]. Many discussions have since taken place on the dynamic behavior of cross-bridges based on the change in a few of the small-angle equatorial reflections. The changes in electron density, however, have not been definitely interpreted on the basis of established molecular structures, although the electron-density distributions in the axial projection with high resolution have recently been derived in some states of muscles [11–13]. We have studied crab muscle by electron microscopy and X-ray diffraction to elucidate the cross-sectional structure with high resolution and have tried to explain the changes in the axial projection of electron-density distribution in the relaxed and rigor states quantitatively.

In this paper, we report our detailed results on the structure of crab striated muscle projected onto the plane normal to the fiber axis. We determined the plausible electron-density maps in the relaxed and rigor muscles with the help of electron microscopy and estimated the amount of mass transfer from the thick to the thin filaments

0301-4622/82/0000–0000/$02.50

when the crab muscle changed from the relaxed to the rigor state. It will be shown that the estimated mass transfer is consistent with the proposed structures for the thin and thick filaments of crab muscle by X-ray layer-line analysis. These results have been briefly reported earlier [14,15].

The crab muscle used in our studies is cross-striated, similar to vertebrate skeletal and insect flight muscles. The sarcomere length (5.5 μm) at rest is longer than those of vertebrate skeletal muscles. The thin filament is formed from actin, tropomyosin and troponin, and the thick filament is formed chiefly from myosin and paramyosin.

2. Materials and methods

2.1. Muscle specimens

Striated muscle from the hind leg of the marine crab, *Portunus trituberculatus*, was used for this study.

Fibers were dissected from the white part of leg muscles. Living relaxed fibers (whole muscle) were immersed in chilled Ringer's solution containing 510 mM NaCl, 12.9 mM KCl, 11.8 mM $CaCl_2$, 23.6 mM $MgCl_2$ and 2.6 mM $NaHCO_3$ (pH 7.2) [16]. Glycerination of the fibers was promoted at the sarcomere length of about 5.5 μm by immersing in 50% glycerol/water containing 1 mM EGTA buffered with 10 mM Tris-maleate (pH 7.0) at -15°C for more than 2 weeks. A single fiber or a bundle containing 2–5 single fibers was immersed in rigor or relaxing solution and used as specimens for X-ray diffraction. The thickness of a single fiber was 300 μm. The composition of the rigor solution was 100 mM KCl, 10 mM $MgCl_2$, 1 mM EGTA and 10 mM histidine · HCl (pH 7.0). Relaxing solution was prepared by adding 10 mM Na_2ATP to the rigor solution.

The sarcomere length of the muscle was measured from light-diffraction patterns using an He-Ne gas laser (NEC, GLG-2026, Tokyo). It was determined as 5.5 ± 0.3 μm. Observation with a phase contrast microscope (Olympus Model FHT-533) confirmed that the length of the A-band occupied 70–80% of the length of 5.5 μm.

2.2. Electron microscopy

2.2.1. Sectioned preparation of muscles

Glycerinated fibers were fixed by immersion in 1% glutaraldehyde in 10 mM cacodylate buffer (pH 7.0). They were post-fixed in 3% osmium tetroxide in the same buffer. The fixed fibers were dehydrated through increasing concentration of ethanol and then propylene oxide. They were embedded in Epon resin. Staining was done with 1% uranyl acetate (pH 7.0) before dehydration by ethanol. Thin transverse sections were cut on a Porter-Blum MT-1 ultramicrotome.

2.2.2. Negatively stained preparation of thick filaments

Filament suspensions isolated from living muscles were prepared by the method of Szent-Györgyi et al. [17]. Filaments were finally suspended in relaxing solution. A drop of the filament suspension was placed on a carbon-coated specimen grid and the filaments were negatively stained with 1% uranyl acetate.

All specimens were examined in a Hitachi HU-11ES electron microscope. The magnification was calibrated by using Dow polystyrene latex particles.

2.2.3. X-ray diffraction

The fibers were attached tightly to the specimen holder in an acrylic plastic cell. The cell has two thin Mylar windows allowing the X-rays to pass through. The specimen holder was cooled to 4°C with a Coolnics thermoelectric cooler (Komatsu-Yamato, Tokyo). Chilled rigor or relaxing solution for glycerinated fibers and chilled oxygenated Ringer's solution for living muscles were circulated in the cell with a peristaltic pump during X-ray exposure.

The X-ray source was a Rigaku-Denki microfocus rotating-anode generator with a copper target (type FR) operated at 50 kV with a tube current of 70 mA. The focus size, viewed at an angle of 6°, was $\approx 100 \times 100$ μm. A mirror-monochromator camera of the type described by Huxley and Brown [1] was made in our laboratory and used to obtain small-angle equatorial diffraction patterns. The curved glass mirror (Spectrosil, vitreous silica) was

placed at 15 cm from the source and the bent germanium monochromator (5°-cut to (111)) was placed at 15 cm from the mirror. Three slits were used to define the beam and to eliminate parasitic scattering. A vacuum tube, enclosing most of the X-ray path, was used to avoid air scattering. The size of the X-ray focus on the film which contains only CuKα_1 radiation ($\lambda = 1.5405$ Å) was about 100×200 μm. Diffraction patterns were recorded on Sakura cosmic-ray films with a film factor of 2.88. Four films were packed in a film cassette to cover a wide range of intensity. Specimen-to-film distance was 45.0 cm.

2.2.4. X-ray intensity data

The optical density of the film was measured with a densitometer (Nalumi type C, Tokyo). Scanning was done along the equator. Data of the optical density sampled at an interval of 10 μm on the film were transferred to a PDP11/34 computer, and they were converted to the scattered X-ray intensity according to the standard scale. Background was subtracted from the intensity curve by assuming a monotonic decrease as the reciprocal radial coordinate R increases (see later fig. 2). Reflections with close spacings were separated by estimating the width of the reflection relative to that of the direct beam. The area under the peak was adopted as an integrated intensity. Lorentz corrections were applied to the intensities by multiplying each intensity by the appropriate R.

2.2.5. Calculations

Calculations were carried out on the PDP11/34 computer.

3. Results and discussion

3.1. Electron microscopy

An electron micrograph of the transverse section of the crab leg muscle in rigor [14] showed an appearance quite similar to that observed in the muscle of another species of crab (*Plagusia dentipes*) by Maéda [18]. Since there was no essential difference between the two different muscles, we mention here briefly our result in conjunction with an X-ray analysis described in section 3.3. Thick filaments were arranged in a hexagonal array and three thin filaments were located in an area surrounded by three thick filaments. The array of these thin filaments was in reverse configuration to that of the surrounding three thick filaments. The diameter of the thick filament was between 20 and 22 nm and that of the thin filament between 7 and 9 nm. The ratio of the number of thin-to-thick filaments in the unit cell is 6. A non-staining core in the center of the thick filament was also observed in the electron micrograph of the overlap region. The diameter of the core is ≈ 7 nm. Such an appearance of the thick filament in cross-section has been often observed in other invertebrate striated muscles [18–22]. This appearance indicates either that no proteins occupy the core or that a protein which has different staining properties from those of myosin is present there. We cannot determine whether or not the non-staining core is hollow, since the sectioned materials are positively stained. So the negative staining technique was applied to isolated thick filaments.

Fig. 1 shows an example of the electron micrographs of negatively stained thick filaments. The micrograph reveals that the axial dense hollow runs down the center of the thick filaments similarly to TMV particles [23]. This indicates that the stain penetrated into the central portion of the thick filaments and that the non-staining core observed in cross-section is a hollow core.

These features of electron micrographs were taken into account for selection of possible Fourier maps in section 3.3.

3.2. Equatorial diffraction patterns

X-ray equatorial diffractions of crab striated muscles were done at the sarcomere length of about 5.5 μm in the relaxed and the rigor states. Relaxed fibers of glycerinated crab muscle did not give the distinct reflections as in rigor muscles and higher order reflections were much more diffuse, indicating disorder in the lattice. Thus, we used living muscles to analyze the cross-sectional structure of the muscle in the relaxed state.

In both states, ten reflections were observed up

Fig. 1. Electron micrograph of negatively stained thick filaments isolated from crab muscle (*Portunus trituberculatus*). The hollow core of the backbone is densely stained with uranyl acetate. Magnification, ×110000.

to a spacing of about 12 nm. Beyond this region, reflections were very weak and diffuse. Fig. 2 shows the intensity curves which were derived from densitometric tracing of X-ray films; curve (a) shows the intensities of reflections from a relaxed muscle and curve (b) those of reflections from a rigor muscle. In curve (b) all peaks were indexed on a hexagonal lattice of lattice spacing (defined by $2/\sqrt{3} \times$ spacing of the 1,0 reflection) 61 ± 1 nm as indicated in fig. 2. The relaxed pattern shows the same reflections as in rigor; the lattice spacing was unchanged within ± 1 nm, but higher order reflections in the range of $0.06\ \text{nm}^{-1} < R < 0.095\ \text{nm}^{-1}$ were less resolved. Unfortunately, thus far we have not been able to obtain patterns of higher quality than the present one. Therefore, referring

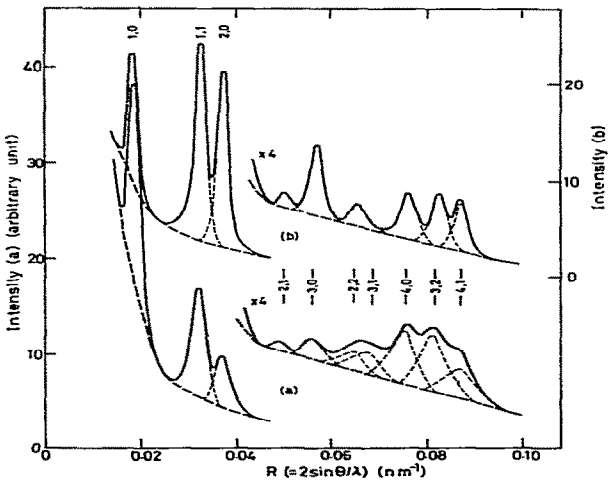

Fig. 2. Equatorial X-ray intensity profiles of crab muscle as a function of R ($=2 \sin\theta/\lambda$, where 2θ and λ are the diffraction angle and the wavelength of X-rays (1.5405 Å)). (a) Relaxed muscle, (b) rigor muscle. Peaks are indexed on Miller indices h, k of a hexagonal lattice with a lattice spacing 61 ± 1 nm. Dashed line, the background; thin dashed line, the profile of the reflections (see text).

to the rigor pattern, reflections were separated by considering their widths which were increased with increase in R as shown in fig. 2.

We have not found additional reflections which seem to come from the thin filament lattice adjacent to or in the Z-line as observed in the vertebrate skeletal muscles [24]. Elliott et al. [25] suggested that the equatorial reflections indexed on a hexagonal lattice are caused by the A-band lattice. In crab muscles, the A-band occupies 70–80% of the sarcomere length of 5.5 μm and the overlap region occupies 95% of the A-band [4]. Thus, the present equatorial reflections arise mostly from the overlap region of the thick and the thin filaments.

In both relaxed and rigor muscles, the 1,0, 1,1 and 2,0 reflections were markedly strong as compared to the wider-angle reflections. This feature differs from those observed in vertebrate skeletal muscles where the 2,0 reflection is very weak at the rest length of sarcomere (e.g. ref. [12]) and in insect flight muscle where the 1,1 reflection is weak (e.g. ref. [26]). These differences reflect the different arrangement of the thin filaments in the lattice from vertebrate and insect flight muscles. As shown in fig. 2, the relative intensities of these inner three reflections are markedly different in the relaxed and rigor states. In the relaxed state, the integrated intensity (uncorrected) of the 1,1 reflection is about two times greater than that of the 2,0 reflection and the 1,0 reflection has almost the same intensity as the sum of the 1,1 and 2,0 reflections. In the rigor state, the 1,1 and 2,0 reflections have almost equal intensity, and their sum is about four times greater than that of the 1,0 reflection. The decrease in the intensity ratio of the 1,0 to the 1,1 or the (1,1 + 2,0) reflections when crab muscle changes from the relaxed to the rigor state is quite similar to the change in other muscles [2,11,21,26,27]. This has been interpreted in terms of the movement of myosin projections where they can attach to and interact with the thin filaments [9]. Namba et al. [4,7] showed in crab muscle that the myosin heads attach to the thin filaments in accordance with the symmetry of the thin filament in the rigor state as in other crustacean muscles [6] and in insect flight muscle [5].

In the next sections, we derive the structures projected along the fiber axis of muscle in the relaxed and rigor states and estimate how much mass associated with a thick filament in the relaxed state is transferred to the thin filaments when the muscle goes into rigor.

3.3. Electron-density distributions in the axial projection

In order to derive the electron-density distributions projected along the fiber axis of muscle in the relaxed and rigor states, Fourier syntheses were calculated using the relative intensities of ten reflections to a resolution of about 7 nm. In the calculation, we adopted the average intensities of reflections from several independent diffraction patterns. The relative values of $|F(hk)|$ ($= I(hk)^{1/2}$, where $I(hk)$ denotes an integrated intensity after the Lorentz correction) of these ten reflections are given in table 1.

Assuming that the projection of the structure along the fiber axis has center of symmetry and that the (1,1) plane is a mirror plane, all combinations of phases (0 or π) for the reflections were tried and two-dimensional Fourier maps were constructed. Among a number of maps obtained, we chose several possible maps by taking into account the observed features of electron micrographs of crab muscle described in section 3.1.

There were five distinct maps in the relaxed state and two maps in the rigor state which correlated well with the features of electron micrographs. They are shown in fig. 3, in which two of five maps chosen for the relaxed muscle are depicted in (a) and (b).

Phases for $|F(hk)|$ assigned in seven Fourier syntheses are given in table 1. All these maps show large areas of high electron density on the lattice points and twelve smaller areas at positions around them. They indicate the electron-density distributions of the thick and the thin filaments, respectively. The profile of the high electron-density region on the lattice point is almost unaltered in the relaxed and the rigor muscles. Thus, the electron-density distribution on the lattice point would describe the structure of the thick filament backbone, indicating that the thick filament backbone has a nearly smooth cylindrical surface. In the maps of fig. 3 (a) and (b), a relatively high elec-

Table 1
Amplitudes and phases of observed h, k reflections in fig. 2

$|F(hk)|$ values were determined as $I(hk)^{1/2}$, where $I(hk)$ values are integrated intensities after the Lorentz corrections. All values of $|F(hk)|$ are expressed relative to $|F(10)|$ normalized to 100. α_{hk} denotes phases used for Fourier syntheses. (x_1), (x_2) and (x_3) are for the Fourier syntheses in which electron-density distribution of myosin heads appeared to have a hexagonal symmetry (see text).

Reflections (h, k)	Relaxed muscle						Rigor muscle		
	$\|F(hk)\|$	α_{hk}					$\|F(hk)\|$	α_{hk}	
		(a)	(b)	(x_1)	(x_2)	(x_3)		(c)	(d)
1,0	100	0	0	0	0	0	100	0	0
1,1	107	0	0	0	0	0	191	0	0
2,0	79	0	0	0	0	0	190	0	0
2,1	8	π	0	π	π	0	25	π	0
1,2	8	π	0	π	π	0	25	π	0
3,0	35	π	π	0	π	0	76	π	π
2,2	43	π	π	π	0	π	55	π	π
3,1	29	0	0	0	0	0	0	–	–
1,3	29	0	0	0	0	0	0	–	–
4,0	70	π	π	π	π	π	76	π	π
3,2	59	π	π	π	π	π	66	π	π
2,3	59	π	π	π	π	π	66	π	π
4,1	35	π	π	π	π	π	51	π	π
1,4	35	π	π	π	π	π	51	π	π

tron-density region centered at a radius of 19.6 nm from the thick filament axis is observed. This is not observed in the maps of rigor muscle. This region is assumed to correspond to the positions of myosin projection of the thick filaments in the relaxed state. The electron-density distribution corresponding to myosin projections has cylindrical symmetry in fig. 3(a) and (b). On the other hand, in the other three maps (not shown here, their phases are given in table 1) it has hexagonal symmetry [15]. From the X-ray layer-line analysis, the symmetry of the structure of the thick filament in crab muscle has been determined by us [15,28]. According to the *n-l* diagram derived by us, the axial projection of the thick filament has a 28-fold rotational symmetry and the first non-zero order of the Bessel function (J_{28}) contributing to the equator occurs at the radial coordinate of about 0.23 nm^{-1}, far away from the region of observed equatorial reflections [15]. Thus, the projection of the structure of the thick filament along the fiber axis should have cylindrical symmetry when derived at the present resolution. Therefore, we considered that the maps of fig. 3(a) and (b) for the relaxed muscle and those of fig. 3(c) and (d) for the rigor muscle describe the plausible electron-density distributions in the axial projection. As shown in table 1, only the phases of the 2,1 reflection differ from each other in these sets of Fourier maps. The Fourier maps of fig. 3(a) and (b) for the relaxed muscle are almost the same, since the contribution of the 2,1 reflection to the Fourier synthesis is small due to the small value of $|F(21)|$. In the rigor muscle, there exists a certain difference between the maps of fig. 3(c) and (d), since $|F(21)|$ is larger as compared with that of the relaxed muscle. The electron density of the thick filament core in fig. 3(d) is considerably higher than in fig. 3(c).

We could not determine a unique solution with respect to the phase experimentally. We were obliged to confine the value of phase based upon the assumptions of center of symmetry in axial projection and the mirror symmetry for the (1,1) plane and to select the plausible maps with the help of electron micrographs and X-ray layer-line analysis. As stated above, in the crab muscle, the arrangement of the thin filaments around the thick filament has center of symmetry. The projection of structure of the thick filament has cylindrical sym-

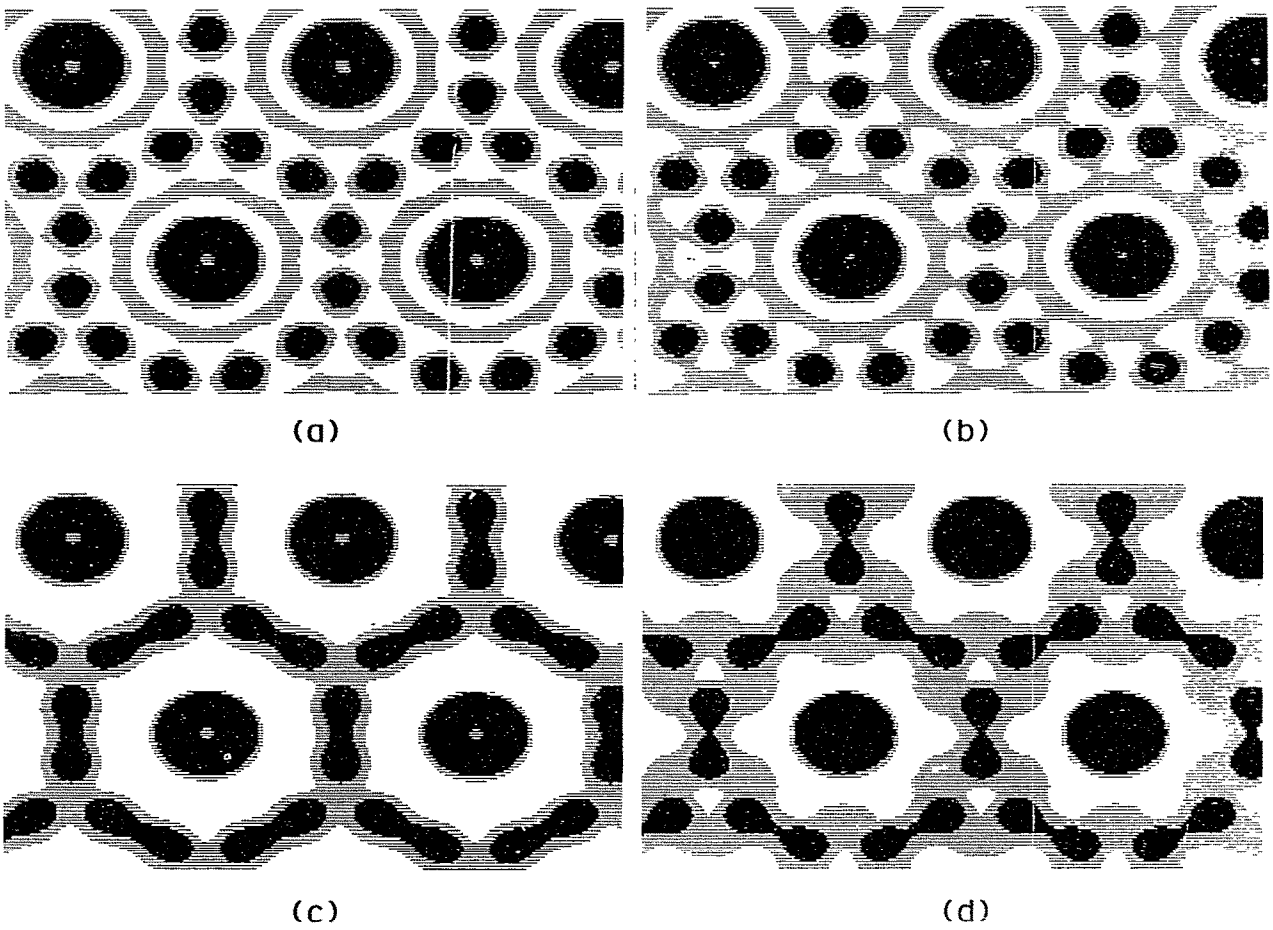

Fig. 3. Two-dimensional Fourier maps. (a) and (b), the maps for the relaxed muscle; (c) and (d), for the rigor muscle. Phases for the structure amplitudes used in these Fourier syntheses are given in table 1.

metry. The thin filament does not have a cylindrically symmetrical structure, but for the more detailed structure, resolution of data greater than that (7 nm resolution) at present is needed. Thus, the assumptions made in the calculation seem to be reasonable at the present limited resolution. The set of phases in fig. 3(a) (or (b) except for the 2,1 reflection) of the relaxed muscle was the same as that of relaxed crab muscle given by Yagi and Matsubara [13] from their calculation of hollow-cylinder thick filaments and the Fourier maps of fig. 3(a) and (b) are very similar to that of Yagi and Matsubara. As will be described in the next section, if we assume that the backbone structure of the thick filaments does not change in the relaxed and the rigor muscles, we can regard fig. 3(a) (or (b)) and fig. 3(c) as representing the best plausible Fourier maps for the relaxed muscle and the rigor muscle, respectively.

3.4. Structural changes and structure parameters

We tried to describe the electron density on an absolute scale. Several diffraction patterns were

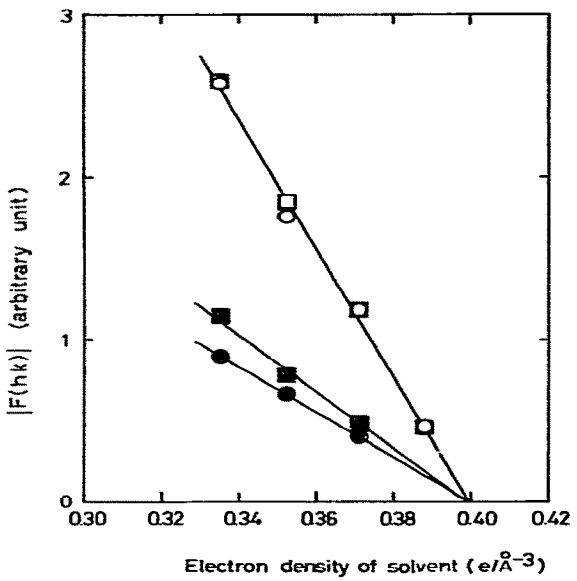

Fig. 4. Changes of $|F(hk)|$ with the electron density of solvent, which was varied by adding glycerol. ○, $|F(11)|$; □, $|F(20)|$; ●, $|F(30)|$; ■, $|F(32)|$.

taken using the same glycerinated rigor muscle, but changing the electron density of the solvent in which the muscle fiber was immersed by adding glycerol. We obtained integrated intensities for the 1,1, 2,0, 3,0 and 3,2 reflections after correcting for absorption of X-rays by the solvent. The relative $|F(hk)|$ values of these reflections were plotted against the electron density of the solvent (fig. 4). They decreased linearly with increase in the electron density of the solvent, and coincided at a value of 0.40 e/Å^3 when extrapolated to the abscissa. The other reflections were weak, but changed in intensity similarly to these four reflections. This result shows that the solvent penetrated into the low electron-density core of the thick filament, and that the mean electron density of the constituent proteins of myofilaments is about 0.40 e/Å^3.

In the electron-density distributions of fig. 3 expressed in an arbitrary scale, the electron density of the outer part of the thick filament was greater than that of the thin filament. The electron density projected along the fiber axis is the averaged electron density, so that it depends on the manner of packing of the constituent molecules in the filaments. The layer-line diffraction pattern from the rigor muscle revealed many distinct reflections due to the thin filaments and a weak remnant of the stronger reflections due to the thick filaments in the pattern from the relaxed muscle [4,7], suggesting that the constituent molecules are packed most densely in the outer part of the thick filament backbone. Therefore, we assumed that the maximum electron density of the thick filament in the Fourier maps is equal to the mean electron density 0.40 e/Å^3. Ripples due to the termination effect in the lowest region in the maps of fig. 3(c) and (d) were smoothed, and this was assumed to be the density level 0.34 e/Å^3 of the solvent (i.e., the rigor solution) in between filaments. In the relaxed muscle, we used living muscles and could not change the density level of solvent within the muscle fibers, since the muscle fibers are surrounded by sarcolemma. As the density level of sarcoplasma in the living muscle may be higher than that of the solvent in the glycerinated muscle, it is not easy to make quantitative comparison between the map of rigor muscle and that of relaxed muscle directly. As mentioned previously, the solvent penetrates into the hollow core of the thick filament and so the profile of the electron density would be uniformly reduced only in the ordinate direction (i.e., the density height) with increase in the density level of solvent. Therefore, assuming that the backbone structure of the thick filaments does not change in the rigor and relaxed muscles, the scaling of both density maps was done so as to make the maximum density and the lowest density of the core in the thick filament backbone coincide. This procedure corresponds to the scaling of the density levels of solvents in the relaxed and rigor muscles, allowing quantitative comparison of changes of electron-density distribution between the relaxed and rigor maps. Fig. 5 shows the comparison of the electron-density distributions along the plane through the centers of the thick and the thin filaments, described on an absolute scale.

Two combinations of fig. 3(a) and (c) and fig. 3(b) and (c) satisfied the assumption that the

structure of the thick filament backbone remained unaltered in the relaxed and the rigor muscles when the above-mentioned scaling was applied. In the combinations of fig. 3(a) and (d) and fig. 3(b) and (d), the outside troughs of the thick filament backbone around the radial positions of about 15 nm (corresponding to ±15 nm in fig. 5) are much deeper in the rigor muscle than in the relaxed muscle. Alternatively, when the scaling was done so as to make the maximum density and the density of the outside troughs of the thick filament backbone coincide, the density level of the thick filament core was about two times higher in the rigor muscle than in the relaxed muscle, while this scaling gave the same result as in the previous scaling in the combinations of fig. 3(a) and (c) and fig. 3(b) and (c). As mentioned already in section 3.3, the maps of fig. 3(a) and (b) have almost the same appearance, and the comparison in fig. 5 is done using the maps with the same phase combination, i.e., fig. 3(a) and (c). The solid-line curve denotes the electron-density distribution of the relaxed muscle taken from fig. 3(a) and the dashed-line curve that of the rigor muscle taken from fig. 3(c). As shown in fig. 5, the electron-density profiles within a radius of about 10 nm from the center of the thick filament are unchanged in both muscles, corresponding to the thick filament backbone. The peak densities of the thin filaments coincide with each other (i.e., 0.38 e/Å^3). The differences between the relaxed and the rigor muscles are the electron densities in the region centered at a radius of 19.6 nm from the center of the thick filament and in the thin filaments. As mentioned previously, the relatively high electron-density region around a radius of 19.6 nm in the solid-line curve corresponds to the position of myosin projections in the relaxed state. The myosin projections lie just between the surface of the thick filament backbone (radius about 10.5 nm) and the surface of the thin filament (radius about 4.2 nm), having a radial width of 6–11 nm. Fig. 5 shows that mass corresponding to myosin projections was transferred to the thin filaments,

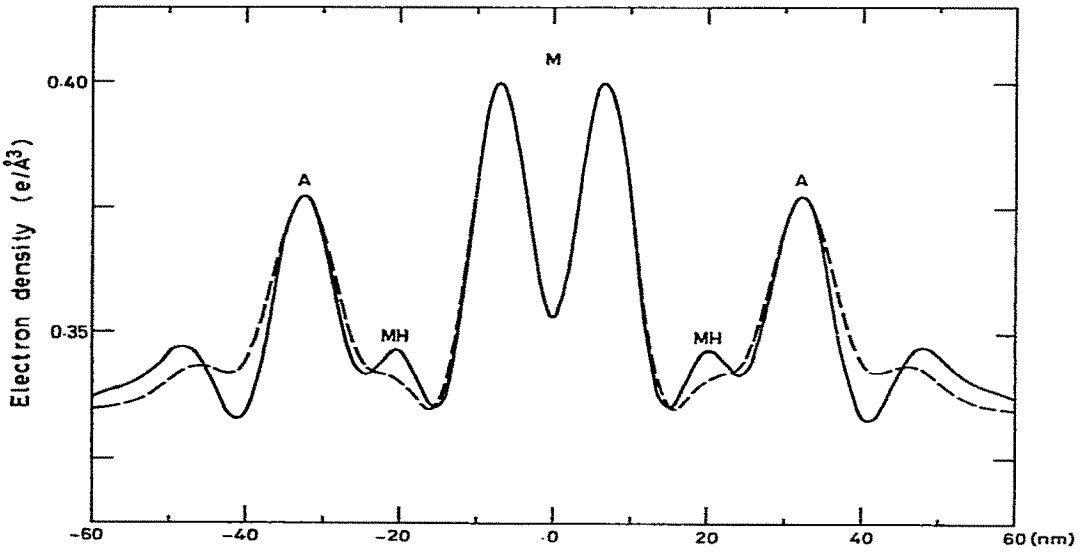

Fig. 5. Electron-density distributions along the plane through the center of the thick and the thin filaments, expressed in an absolute scale. Solid-line curve, the relaxed muscle corresponding to fig. 3(a); dashed-line curve, the rigor muscle to fig. 3(c). The scaling was done so as to make the maximum density and the lowest density of the core in the thick filament backbones coincide. A, thin filament; M, thick filament; MH, myosin head.

causing slightly larger spread of the electron density of the thin filaments in the rigor state. Namba et al. [4,7] derived the structure of the thin filament in the crab muscle from the analysis of the layer-line diffraction patterns. The cylindrically averaged electron density of the thin filament projected along the fiber axis was calculated from their model in the rigor state at 7 nm resolution, and this was found to be similar to that obtained from the present equatorial analysis. Therefore, small spread of the electron density of the thin filament in the dashed-line curve of fig. 5 is consistent with the previous result such that the myosin heads are attaching tightly to and incorporated in the thin filaments in the rigor state [4,7].

In table 2 are summarized the structural parameters of the relaxed and rigor muscles determined from the Fourier syntheses. The diameter of the thick filament backbone estimated from the width at the half maximum of the profile was 21–22 nm, which is much larger than that of vertebrate skeletal muscles [29,30] but is comparable to that of other crustacean muscles [3,13]. The diameter of the low electron-density core of the thick filament was about 7 nm. Thus, the rod portions (light meromyosins) of myosin molecules would pack into a surface layer of the backbone of thickness about 6–7 nm.

3.5. Estimation of mass transfer

In order to estimate the mass transfer from the thick filaments to the thin filaments when the muscle goes from the relaxed to the rigor state, we evaluated the amount of mass associated with the thick filament and the thin filament in the Fourier maps. In the Fourier maps corresponding to fig. 5, the volumes above the lowest level were measured within a radius of 15 nm from the filament axis for the thick filament backbone, within the region between a radius of 15 and 22.5 nm for the part of myosin projections and within a radius of 6.3 nm from the filament axis for the thin filament. In table 3, these values are normalized so that the mass of the thick filament backbone is unity.

From these values, the increase of mass per six thin filaments in the rigor muscle is $(0.16 - 0.11) \times 6 = 0.3$. This is very close to the mass (0.26) of myosin projections of a thick filament in the relaxed muscle. In the structure of the thin filament of crab muscle derived from the X-ray layer-line analysis [4], the molecular weight of the thin filament per 38.2 nm in the relaxed muscle is 92.8×10^4; molecular weights of the constituent molecules used in the calculation are 4.2×10^4 for actin, 7.0×10^4 for tropomyosin and 10.0×10^4 for troponin. By reference to this value, the in-

Table 2
Structural parameters determined by Fourier syntheses

Diameter was determined from the width at half maximum of profile. For the radial width of myosin head, the width at half maximum (hw) and the full width (fw) are given.

Distance (nm)	Thick-to-thick filaments	61.4	
	Thick-to-thin filaments	31.7	
	Thin-to-thin filaments	16.3	
	Myosin head-to-thick filament	19.6	
	Myosin head-to-thin filament	12.1	
Diameter (nm)		Relaxed	Rigor
	Thick filament backbone	21.0	21.9
	Thick filament core	6.9	6.8
	Thin filament	8.4	9.5
Radial width of myosin head (nm)		6.0 (hw)	–
		10.6 (fw)	–

Table 3
Relative mass estimated from Fourier maps

Values are normalized so that the mass of the thick filament backbone in the relaxed muscle is unity.

	Relaxed	Rigor
Thick filament backbone (within 15 nm in radius)	1.0	1.05
Part of myosin head (within 15–22.5 nm in radius)	0.26	0.17
Thin filament (within 6.3 nm in radius)	0.11	0.16

crease in the molecular weight of the thin filament per 38.2 nm which is a half period of the thin filament is estimated as $92.8 \times 10^4 \times (0.16 - 0.11)/0.11 = 42.2 \times 10^4$, corresponding to 4 myosin subfragment-1 (S1) of molecular weight 10×10^4 [31]. This result is in quite good agreement with our model of the thin filament in rigor [4]. From the relative mass to the thin filament in the relaxed muscle, the total molecular weight of myosin projections per 14.5 nm (which is the axial repeat of the thick filament of crab muscle [4]) along the thick filament is estimated as $92.8 \times 10^4 \times (0.26/0.11) \times (14.5/38.2) = 83.3 \times 10^4$. Although the molecular weight of myosin subfragment-2 (S2), which is the linkage between myosin heads (S1) and light meromyosin, is fairly large, it has a fine and long filamentous structure [31]. If we assume that the portion of myosin projections in the Fourier maps corresponds to the localization of S1, eight S1 would be contained in that portion. This suggests that there would be no more than four projections on every 14.5 nm level along the thick filament, implying that the thick filament of crab muscle has a four-stranded structure. This is consistent with the helical symmetry of the thick filament derived from the analysis of layer-line reflections [15,28]. The number of S1 around the thick filament backbone in the relaxed state is in fair agreement with that of S1 bound to the thin filament in the rigor state.

Acknowledgements

We are grateful to Professor T. Mitsui for discussions, and Dr. B.M. Millman (University of Guelph, Canada) for critical reading and helpful comments at an earlier stage of this paper.

References

[1] H.E. Huxley and W. Brown, J. Mol. Biol. 30 (1967) 383.
[2] A. Miller and R.T. Tregear, J. Mol. Biol. 70 (1972) 85.
[3] J.S. Wray, P.J. Vibert and C. Cohen, Nature 257 (1975) 561.
[4] K. Namba, K. Wakabayashi and T. Mitsui, J. Mol. Biol. 138 (1980) 1.
[5] K.C. Holmes, R.T. Tregear and J. Barrington Leigh, Proc. R. Soc. Lond. B207 (1980) 13.
[6] J.S. Wray, P.J. Vibert and C. Cohen, J. Mol. Biol. 124 (1978) 501.
[7] K. Namba, K. Wakabayashi and T. Mitsui, in: Cross-bridge mechanism in muscle contraction, eds. H. Sugi and G.H. Pollack (University of Tokyo Press, Tokyo, 1979) p. 445.
[8] Y. Maéda, I. Matsubara and N. Yagi, J. Mol. Biol. 127 (1979) 191.
[9] H.E. Huxley, J. Mol. Biol. 37 (1968) 507.
[10] J.C. Haselgrove and H.E. Huxley, J. Mol. Biol. 77 (1973) 549.
[11] J. Barrington Leigh and G. Rosenbaum, Annu. Rev. Biophys. Bioeng. 5 (1976) 239.
[12] J.C. Haselgrove, M. Stewart and H.E. Huxley, Nature 261 (1976) 606.
[13] N. Yagi and I. Matsubara, J. Mol. Biol. 117 (1977) 797.
[14] K. Wakabayashi and K. Namba, Proc. 6th Int. Biophys. Congr. Kyoto Abstr. (1978) 381.
[15] K. Wakabayashi and K. Namba, in: Protein dynamics and energy transduction, ed. S. Ishiwata (Taniguchi Found., 1980) p. 478.
[16] P. Fatt and B. Katz, J. Physiol. 120 (1953) 171.
[17] A.G. Szent-Györgyi, C. Cohen and J. Kendrick-Jones, J. Mol. Biol. 56 (1971) 239.
[18] Y. Maéda, Eur. J. Biochem. 90 (1978) 113.
[19] J. Auber and R. Couteaux, J. Microscopie 2 (1963) 309.
[20] B. Bullard, K.S. Hammond and B.M. Luke, J. Mol. Biol. 115 (1977) 417.
[21] B.M. Millman and P.M. Bennett, J. Mol. Biol. 103 (1976) 439.
[22] E.W. April, P.W. Brandt and G.F. Elliott, J. Cell Biol. 51 (1971) 72.
[23] S. Brenner and R.W. Horne, Biochim. Biophys. Acta 34 (1959) 103.
[24] G.F. Elliott, J. Lowy and B.M. Millman, J. Mol. Biol. 25 (1967) 31.
[25] G.F. Elliott, J. Lowy and C.R. Worthington, J. Mol. Biol. 6 (1963) 295.

[26] R.S. Goody, K.C. Holmes, H.G. Mannherz, J. Barrington Leigh and G. Rosenbaum, Biophys. J. 15 (1975) 687.
[27] J.S. Wray, P.J. Vibert and C. Cohen, J. Mol. Biol. 88 (1974) 343.
[28] K. Namba, K. Wakabayashi and T. Mitsui, 18th Ann. Meet. Biophys. Jap. Abstr. (1980) 170.
[29] H.E. Huxley, in: The structure and function of muscle, Vol. 1, ed. G.H. Bourne (Academic Press, London, 1972) p. 301.
[30] J.M. Squire, J. Mol. Biol. 77 (1973) 291.
[31] S. Lowey, H.S. Slayter, A.G. Weeds and H. Baker, J. Mol. Biol. 42 (1969) 1.